NANO LETTERS

pubs.acs.org/NanoLett

Cooperative Adhesion and Friction of Compliant Nanohairs

Liehui Ge,[†] Lijie Ci,[‡] Anubha Goyal,[‡] Rachel Shi,[†] L. Mahadevan,[§] P. M. Ajayan,[‡] and Ali Dhinojwala*[,†]

[†]Department of Polymer Science, The University of Akron, Akron, Ohio 44325, United States, [‡]Department of Mechanical Engineering and Materials Science, Rice University, Houston, Texas 77005, United States, and [§]School of Engineering and Applied Sciences, Harvard University, Cambridge, Massachusetts 02138, United States

ABSTRACT The adhesion and friction behavior of soft materials, including compliant brushes and hairs, depends on the temporal and spatial evolution of the interfaces in contact. For compliant nanofibrous materials, the actual contact area individual fibers make with surfaces depends on the preload applied upon contact. Using in situ microscopy observations of preloaded nanotube hairs, we show how nanotubes make cooperative contact with a surface by buckling and conforming to the surface topography. The overall adhesion of compliant nanohairs increases with increasing preload as nanotubes deform and continuously add new side-wall contacts with the surface. Electrical resistance measurements indicate significant hysteresis in the relative contact area. Contact area increases with preload (or stress) and decreases suddenly during unloading, consistent with strong adhesion observed for these complaint nanohairs.

KEYWORDS Carbon nanotubes, adhesion, gecko-inspired materials, friction

The behavior of fibrillar materials has been of significant interest recently due to the fact that these materials have properties that can be tuned by controlling the individual response of the constituent filaments as well as the interactions between them and their density, topology, and order in the network. These fibrillar materials are also beginning to be useful as interfaces due to potential applications as gecko-inspired adhesives[1−5] and responsive surfaces.[6] Understanding the friction and adhesion of these artificially textured surfaces has been difficult because the nature of contact area is not necessarily determined by the end contact but depends both on the cooperative interactions between the filaments and on the anisotropic compliance of the textured interface.[7,8] This is particularly true of fibrillar interfaces since the behavior of the constituent filaments in compression and tension is vastly different; filaments buckle and bend but do not stretch easily. To explore the behavior of these interfaces, here we have used a combination of mechanics, electrical resistance, and in situ scanning electron microscopy (SEM) to understand the contact between hairs of a large number of vertically aligned carbon nanotubes (VA-CNTs) with glass or silicon substrates. We find that these carbon nanotubes do not make end contacts but instead show significant increase in side contacts (and relative contact area) with increase in preload, which we suggest allows us to explain the unusual adhesive and frictional properties of the VA-CNT brushes as a function of preload.

The results of compressing a VA-CNT bundle of 500 μm × 500 μm in size and 280 μm in height (referred to as an array) when loaded at a displacement rate of 1 μm/s) with glass substrates are shown in Figure 1A. The stress−strain curve is highly nonlinear and has three distinct regions during compression. In the first regime, at low strains (less than 5%), the modulus of the VA-CNT is very low but variable (0.3 ± 0.2 MPa). This large variability in the apparent modulus for small strains is due to the polydispersity of nanohair lengths that leads to changes in density of the CNT away from the ends (Figure 2D) and due to the experimental difficulty of aligning the two surfaces to make perfect parallel contact. Both these effects cause all the nanotubes to fully engage with the substrate only when the strain is of the order of 5%, leading to an increase in the apparent modulus. In the second more distinct region (strain of 5−20%) all the carbon nanotubes are engaged and the modulus is 1.6 ± 0.3 MPa. In this regime, we have observed irreversible changes near the interface where the nanotube hair undergoes buckling and consequent adhesion. Finally, beyond a critical stress of order 0.2 MPa, we observe a significant change in slope and the modulus drops to 0.25 ± 0.1 MPa. In this regime, the material deforms with a very small increase in stress due to buckling and bending of the nanotube hairs. The retraction cycle has significant hysteresis with an adhesive jump-out and the height of the nanotube brush is reduced permanently. Since the fibers are oriented, we expect the modulus of the interface to be anisotropic; the modulus perpendicular to the orientation direction of the aligned VA-CNT is 90 ± 20 kPa (Figure 1B), a factor of 18 less than that along the fiber length (the modulus along the fiber length is 1.6 MPa). Furthermore, we see that the stress

* To whom correspondence should be addressed, ali4@uakron.edu.
Received for review: 07/9/2010
Published on Web: 10/12/2010

DOI: 10.1021/nl102398w | *Nano Lett.* **2010,** *10,* 4509–4513

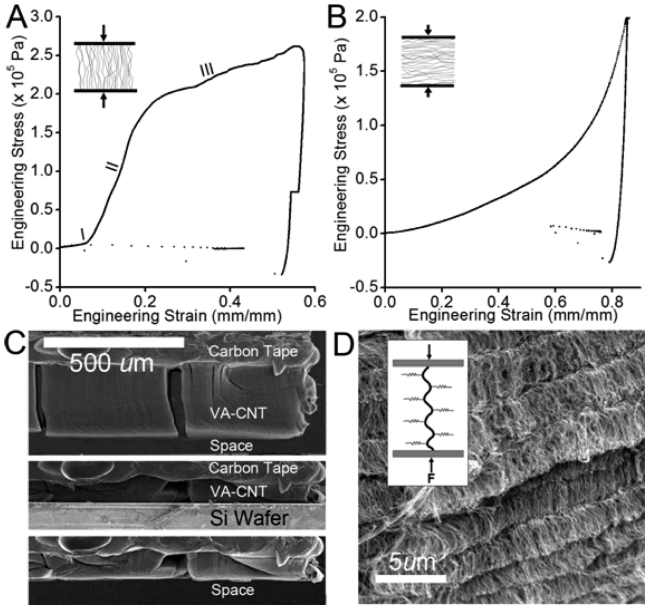

FIGURE 1. Anisotropic compression modulus of multiwalled vertically aligned carbon nanotube array. (A) Stress−strain measurements of a 280 μm tall VA-CNT array parallel to the orientation of the VA-CNTs. (B) The stress−strain curve measured perpendicular to the orientation of the VA-CNTs. (C) Side view scanning electron micrograph of the VA-CNT array before compression (top panel), under compression (center panel), and after compression (lower panel). After the normal load is removed, the height of the VA-CNTs does not recover. (D) SEM image showing the buckling of the VA-CNT array under pressure. The periodicity of the buckling is much larger than the intrinsic undulations. A sketch shows the constrained buckling model where a stiff rod of modulus E is surrounded by a matrix with a modulus G. A compression force initiates buckling. However, a single buckle is inhibited by the surrounding VA-CNTs and this leads to periodic buckling that is not correlated with the height of the VA-CNT array.

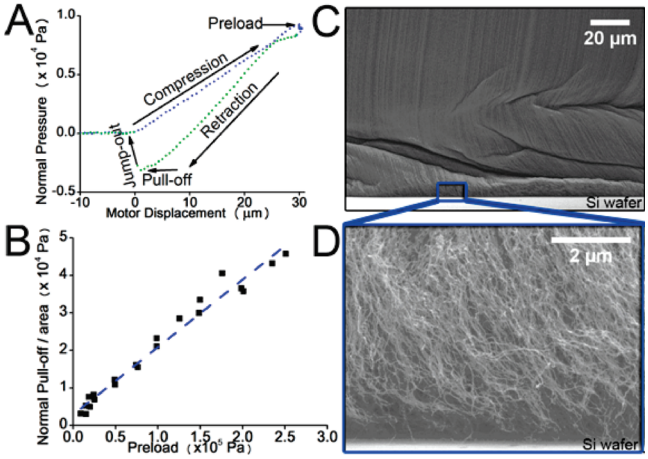

FIGURE 2. Normal pull-off measurements of a VA-CNT array with increasing preload. (A) A typical cycle for adhesion measurements that shows jump-out indicating adhesive contact (≈300 μm in height). (B) Normal pull-off force/area scales linearly with preload (units of pressure). (C) Side view SEM image of the VA-CNT array under compression shows buckling of VA-CNTs close to interface (the bottom substrate is silicon in the SEM images). (D) High-resolution SEM side view image of VA-CNT compression shows that the buckling near the interfaces creates many side contacts of CNTs with the smooth silicon surface.

increases monotonically with deformation and the structure does not recover after unloading, indicating that adhesion between the VA-CNTs prevents recovery. Indeed, there is a sudden pull out as a result of loss of adhesion between the sides of VA-CNTs and the surface (glass), indicating an important role in adhesion.

To visualize the changes taking place during compression (parallel to the orientation of aligned VA-CNTs), we acquired SEM images of the nanotube hair before contact and during compression as shown in Figure 1C. Figure 1C (top panel) shows the SEM image of MWCNT hairs before contact. The nanotube hairs bend under pressure, but these bends recover if the strains are less than 5−10%. At higher strains, the structure deforms significantly under pressure (Figure 1C, center panel). In some of the pillars we observe the formation of kinks which remain on unloading (Figure 1C). This irreversible deformation of the VA-CNTs is analogous to that in the capillary-induced collapse of VA-CNTs[9] due to the mutual adhesion of VA-CNTs. We see that while thin VA-CNTs (8 nm diameter) deform irreversibly, much thicker VA-CNT tubes (40 nm diameter)[10] do recover on unloading, because of the much higher bending stiffness (discussed below) relative to adhesion.

To quantify the role of the individual nanotubes on the properties of the brush, we note that for the 40 nm diameter VA-CNTs, the density of carbon nanotubes is 10^{10} carbon nanotubes/cm^2, and the modulus is 50 MPa. For the 8 nm VA-CNTs, the density is 7×10^{10} carbon nanotubes/cm^2, and the modulus of 1.6 MPa. Normalizing with the number of the tubes/area, the 40 nm diameter VA-CNT tubes have compression modulus of 500 nN/nanotube and the 8 nm diameter VA-CNTs have a compression modulus of 1−2 nN/nanotube, respectively. Since the bending stiffness of hollow tubes is

$$EI = E\pi(d_o^4 - d_i^4)/64$$

where E is Young's modulus, I is the area moment of inertia, d_o is the outer diameter, and d_i is the inner diameter of the tube; the thick tubes should be ≈300 times stiffer than the thin tubes, consistent with the experimental measurements of ≈250−500.

Next we turn to the role of the collective mechanics of the CNTs that form the brush. High-resolution side-view SEM images in Figure 1D show that individual carbon nanotubes are intrinsically wavy structures. Previous attempts to explain the behavior of these arrays rely on the Euler buckling model for isolated fibers,[10−13] according to which the buckling stress scales as $\approx \pi^2 EI/N L_c^2$. Using $E \sim 1 TPa$ (an ideal upper limit for CNT), $N \approx 10^{11}$ carbon nanotubes/cm^2, and length of VA-CNTs ≈300 μm, we obtain the critical stress of 20 Pa. This estimate based on the Euler model is many orders of magnitude smaller than the measured critical stress of 0.2 MPa (Figure 1). In addition, these buckling stresses are not a function of the height of the VA-CNT hairs.[11] This is because one must account for the interactions

DOI: 10.1021/nl102398w | Nano Lett. 2010, 10, 4509–4513

between the VA-CNTs—indeed the fibrillar interface behaves more like an orthotropic material. To understand the response of individual tubes, we assume that each one is surrounded by a soft material of other VA-CNTs with an effective modulus G. The lateral compressibility of the VA-CNT restricts long wavelength buckling and the bending stiffness of VA-CNT prohibits short wavelengths. The balance of these two opposing effects leads to periodic buckling with a wavelength $(\lambda) = 2\pi(\kappa/\alpha)^{1/4}$, where κ is the bending rigidity and $\alpha \approx 2.4$ G.[14,15] For G $\approx 90 \pm 20$ kPa (Figure 1B), we predict $\lambda \approx 1.1$ μm, similar to the values observed in the experiments ($\approx$2−3 μm, Figure 1D).

In addition to increasing the effective stiffness, the cooperative bending and buckling deformation of the VA-CNT also affects the adhesion and friction properties of the brush. Figure 2A shows a typical cycle of loading and unloading of the VA-CNT brush. During retraction a sudden pull-out is observed, indicating loss of adhesive contact (Figure 2A). Figure 2B shows the pull-off forces/area as a function of preload, and we observe that the normal stress increases with increase in preload. In panels C and D of Figure 2, the SEM images of the side wall of the nanotube bundle under preload show significant buckling and increase in adhesive contact at the interface consistent with a cooperative increase in adhesive forces that is quite unlike the response of simple adhesive elastic contacts, where the pull-off forces/area is independent of preload.[16,17]

The combination of anisotropy in the mechanical response and the adhesion of the soft compliant VA-CNT brush also lead to an unusual shear response. We first applied a preload as previously described and then retracted the load until the applied load is close to zero. These measurements are unlike the traditional friction measurements where the shear forces are measured as a function of normal load.[18] The shear measurements at minimal normal load are sensitive to the adhesive forces and hysteresis of the contact after the preload is applied on the sample. Figure 3A shows that the shear force increases uniformly with displacement until the brush slips intermittently via a characteristic stick−slip motion. In Figure 3B, we plot the maximum nominal shear stress as a function of applied preload and observe that it increases with the preload suggesting that this is directly correlated with the adhesion of the hairy array. Interestingly, the shear forces are also a factor of 4 times higher than the normal pull-off measurements, and this anisotropy between the shear and adhesion forces is intrinsic property of fibrillar structures.[3,5,18]

Further evidence for the role of collective behavior of the VA-CNT in controlling adhesion and friction is observed in the SEM images collected before (Figure 3C, top panel) and after the shear experiments (Figure 3C, bottom panel). Initially, before shear, we see that the nanotubes are mostly perpendicular to the surface and form small adhesive clumps. After contact and shear we observe a significant alignment of the VA-CNT with the substrate and a concomitant increase

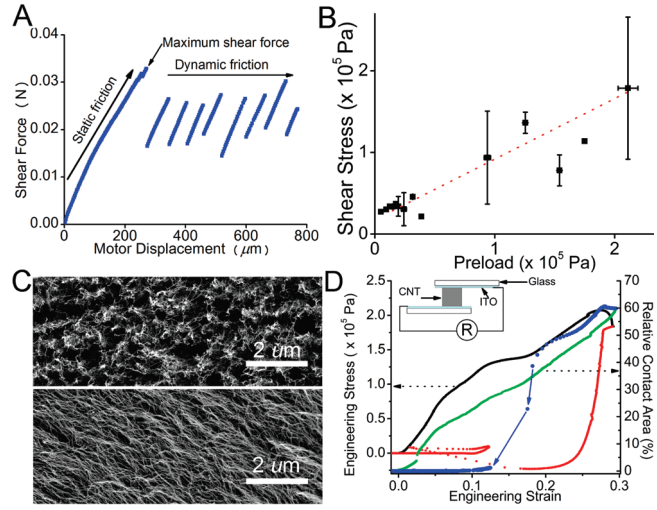

FIGURE 3. Shear measurements of a VA-CNT array with increasing preload. (A) A typical shear profile shows the static friction force buildup until it reaches maximum static shear force. The normal preload is reduced to close to zero after applying normal preload for 5 min. The shear forces are measured under the condition of nearly zero normal load. Stick−slip happens in the dynamic friction region. (B) The critical shear stress when the sample starts to slide is plotted as a function of normal preload (units of pressure). The results for smaller preloads (<50 $\times$ 10^3 Pa) were done on a 500 μm $\times$ 500 μm size array (and 300 μm in height) using the friction cell. The shear stress for larger preloads (>50 $\times$ 10^3 Pa) was measured using 4 mm $\times$ 4 mm (VA-CNT arrays with width of 500 μm $\times$ 500 μm and 100 μm in height) samples. (C) SEM images showing the top view of the surface of the VA-CNT array before contact (upper panel) and after contact (lower panel). (D) Stress (black, loading; red, unloading) and relative contact area (green, loading; blue, unloading) as a function of strain. The inset in Figure 3D shows the setup used to measure the resistance and stress as a function of strain.

in the number of contacts of carbon nanotubes with the surface. Visually, the matted appearance before contact turns to a glossy, shiny appearance after contact consistent with the transition to a smooth aligned surface. The side view of the nanotube brush in contact with a silicon wafer after shear confirms that not only the ends but also the buckles are oriented along the direction of shear.

To determine the contact area as a function of preload, electrical resistance was measured in conjunction with stress−strain measurements. The sample geometry used to measure electrical resistance is shown in Figure 3D as an inset. The Figure 3D shows the stress−strain curve during compression along with the relative contact area (details discussed in the methods section and the raw data for change in resistance as a function of strain are shown in Figure S3 (Supporting Information). Interestingly, the relative contact area increases monotonically as the sample is compressed. During the retraction cycle, the contact area and the mechanical behavior show significant hysteresis. The jump-out at 50% contact area explains why both adhesion and friction forces scale with applied load. The contact area for these compliant nanohairs is a function of applied load, and because of intrinsic adhesion the contact area shows significant hysteresis.

DOI: 10.1021/nl102398w | *Nano Lett.* **2010,** *10,* 4509−4513

From the SEM images in Figure 3C, we can observe that the increase in contact area is due to side contacts of the carbon nanotubes. The average length of the carbon nanotube making side contact is around $1.7 \pm 0.5\ \mu$m. We can also estimate the characteristic length for bending based on the adhesion energy and bending stiffness ($l \approx (EI/\gamma)^{1/2}$.[19] Using $EI \approx 1.7 \times 10^{-22}$ N m^2 and using $\gamma \approx 2.8$ eV/nm,[19] we obtain $l \approx 0.7\ \mu$m, which is similar to the average length of the carbon nanotube making side contacts. Interestingly, the average characteristic length for a 40 nm tube is around 11 μm, and this also explains the difficulty in achieving high adhesion with much stiffer tubes.

In summary, we have demonstrated that the cooperative nature of the compliant nanohairs under load controls its anisotropic mechanical properties, adhesion, and friction. The relative contact area for these nanohairs increases with increase in load and is very hysteretic with no real decrease in the actual area of contact until pull-off. This hysteretic behavior of contact area explains the increase in adhesion and friction forces with applied preload. Understanding the mechanics and deformation of nanoscale fibers such as carbon nanotubes is critical for designing materials for gecko-inspired adhesives, soft resilient foams, nanocomposites, and shape-memory materials.[3−5,10,20−22] The dynamic nature of contact under load made by soft and nanoscale materials and the difficulty in determining their footprints underpin the challenges in understanding nanoscale tribology and adhesion.

Methods. ***Procedure To Grow Carbon Nanotubes.*** The experimental process for the growth of aligned carbon nanotubes involves three steps: photolithography, catalyst deposition, and chemical vapor deposition (CVD) process. After the photolithographic pattern process, an electron beam was used to deposit a 10 nm thick aluminum (Al) buffer layer on a Si or Si/SiO_2 wafer. A 1.5 nm thick iron catalyst layer (which forms nanosized particles for catalytic growth of carbon nanotubes) was deposited on top of the Al layer. The CVD setup to grow carbon nanotubes consists of a tubular furnace with an alumina processing tube (45 mm inner diameter). Aligned carbon nanotubes films were prepared by thermal decomposition of ethylene (with a flow rate of 50−150 sccm) on the catalyst film at 750 °C. An Ar/H_2 gas mixture (15% H_2) with a flow rate of 1300 sccm was used as the buffer gas during the whole CVD run. A very low concentration of water vapor with dew point of 20 °C was carried to the reaction furnace by a fraction of Ar/H_2 flow during carbon nanotube growth. The growth time is 10−30 min, and the length of carbon nanotubes is about 200−500 μm. The average diameter of the carbon nanotubes is 8 nm (two to five walls).

Sample Preparations. The VA-CNT array is transferred from the Si wafer to the 3 mm × 3 mm glass slide in the following steps. First, a thin layer of un-cross-linked PDMS resin is coated on plasma-cleaned glass. The PDMS resin is allowed to cure until it is tacky. Second, the PDMS layer is pressed slightly against the VA-CNT top surface and is placed in the oven at 100 °C for about 1 h for the resin to cure completely. Then the glass slide is peeled off from the wafer with the VA-CNT pillars transferred onto the glass. Unwanted pillars are removed manually with a razor blade under a stereoscope. The sample is then mounted on the friction cell to measure its adhesion and friction response. The samples for electrical measurement were transferred by using silver-filled epoxy paste.

To obtain high-resolution images during contact of VA-CNT with a silicon wafer, charging must be minimized. To prevent charging, we have used silicon wafers sputtered with a thin layer of silver. The VA-CNT array (3 mm × 3 mm) was transferred to a double-sided sticky carbon tape. The other side of the carbon nanotube was mounted on the wafer sputtered with a thin layer of silver. A custom-designed sample holder was used to mount the VA-CNT sample in a SEM chamber. We have collected high-resolution images after bringing the VA-CNT in contact with another blank silver-coated Si wafer. The combination of the conductive carbon tape and silver layer reduced charging.

Mechanical Measurements. Measurements of stress were performed using an MTS Nano Bionix that measured force to $\pm 10\ \mu$N. The adhesion and friction measurements were performed using a home-built friction and adhesion cell that consists of a sample holder with two degrees of freedom (x and y). There are two pairs of low friction linear bearings perpendicular to each other at the bottom of the platform to guide smooth motion in the x and y directions. In each direction, the holder is driven by New Focus picomotors with a resolution of ≈30 nm/step. The exact calibration of this motion is done by using a traveling microscope. There are two sets of wide double cantilever beams perpendicular to each other which isolate the deflection in x and y directions. The deflections of the cantilever beams are measured by two capacitors. The capacitor has one plate mounted on the cantilever and the other on a stationary post. A triangle wave ac current is applied to the capacitors. Deflection of the cantilever beam changes the distance between the two plates resulting in a change in capacitance. The corresponding changes of voltage on the plate capacitors are measured.

The adhesion and friction cell is calibrated by hanging known weights and detecting the changes in the voltage of the capacitors. Two independent capacitors are used to measure the shear and normal forces. The spring constants are measured by bringing the surfaces into contact and by measuring the force as a function of displacement. The calibration curves are linear in the region of forces used in these experiments.

In the case of shear measurements, we were able to use the same samples for multiple measurements for low preloads. However, for higher preloads the shear stresses are high enough to permanently deform the VA-CNT structure during sliding and those arrays were only used once. The

DOI: 10.1021/nl102398w | *Nano Lett.* **2010,** *10,* 4509–4513

shear data for larger preloads were collected on larger arrays of VA-CNT (4 mm × 4 mm size).[3]

Electrical Measurements To Determine Real Contact Area. The electrical resistance of the contact interface was measured simultaneously with the stress−strain measurements. The stress−strain measurements were done using a MTS Nano Bionix instrument. The sample geometry was modified to measure the electric resistance during the loading and unloading cycle. A 500 μm × 500 μm VA-CNT sample is transferred on conductive indium tin oxide (ITO) glass substrate by using silver-filled epoxy. The electrical resistance is measured using a Keithley 2700 digital multimeter after bringing the VA-CNT in contact with an opposite piece of ITO glass substrate. We assume that the total resistance we measured is the sum of resistance of the ITO substrates (R_{ITO}), resistance (R_{CNT}) of carbon nanotube bundle, and the resistance (R_{int}) of the interface. It is also assumed that resistance of the contact interface is inversely proportional to the contact area. The resistance (and maximum achievable contact area) at strain values of 80−90% was taken as minimum resistance of the system ($R_{min} = 95\ \Omega$). The resistance (R_{ITO}) for the direct ITO−ITO contact was 45 Ω. To measure the resistance of the CNT bundle (R_{CNT}), we mounted both ends of the CNT's on copper electrodes using silver-filled epoxy. This way we ensured that the contact resistance at the interface was negligible. R_{CNT} was 9 Ω for a 500 μm × 500 μm patch, and this value was relatively insensitive to the compression of the CNTs. The relative contact area was then determined using the following equation: $(R_{min} - R_{ITO} - R_{CNT})/(R - R_{ITO} - R_{CNT})$.

SEM Imaging. To image a CNT array under normal and shear load, we have designed a miniature version of the friction cell consisting of two holders that sit on two linear bearings perpendicular to each other. With the holders moving along perpendicular directions, it can hold normal and shear load applied to the sample. The motion is driven manually with two microactuators. Average side contact length was obtained by averaging the lengths of 30 randomly selected nanotubes from three SEM images taken at random locations of the top surface. The number density was obtained by counting the number of tubes in a box of 2 μm wide and the same length as the average tube length. The number density before contact was obtained by counting the tube ends in a 2 μm × 2 μm box.

Acknowledgment. We acknowledge the financial support from NSF-DMR-0512156, the Nanoscale Interdisciplinary Research Teams grant from NSF-0609077, and the Harvard-NSF MRSEC. We thank Todd Blackledge (UAkron) for the use of the MTS Nanobionix.

Supporting Information Available. The SEM images of side contacts and plot of electrical measurements. This material is available free of charge via the Internet at http://pubs.acs.org/.

REFERENCES AND NOTES

(1) Autumn, K.; Sitti, M.; Liang, Y. A.; Peattie, A. M.; Hansen, W. R.; Sponberg, S.; Kenny, T. W.; Fearing, R.; Israelachvili, J. N.; Full, R. J. *Proc. Natl. Acad. Sci. U.S.A.* **2002**, *99*, 12252–12256.
(2) Arzt, E.; Gorb, S.; Spolenak, R. *Proc. Natl. Acad. Sci. U.S.A.* **2003**, *100*, 10603–10606.
(3) Ge, L.; Sethi, S.; Ci, L.; Ajayan, P. M.; Dhinojwala, A. *Proc. Natl. Acad. Sci. U.S.A.* **2007**, *104*, 10792–10795.
(4) Yurdumakan, B.; Raravikar, N. R.; Ajayan, P. M.; Dhinojwala, A. *Chem. Commun. (Cambridge, U.K.)* **2005**, 3799–3801.
(5) Qu, L.; Dai, L.; Stone, M.; Xia, Z.; Wang, Z. L. *Science* **2008**, *322*, 238–242.
(6) Pokroy, B.; Kang, S. H.; Mahadevan, L.; Aizenberg, J. *Science* **2009**, *323*, 237–240.
(7) Tang, T.; Hui, C.-Y.; Glassmaker, N. J. *J. R. Soc., Interface* **2005**, *2*, 505–516.
(8) Tian, Y.; Pesika, N.; Zeng, H.; Rosenberg, K.; Zhao, B.; McGuiggan, P.; Autumn, K.; Israelachvili, J. *Proc. Natl. Acad. Sci. U.S.A.* **2006**, *103*, 19320–19325.
(9) Futaba, D. N.; Hata, K.; Yamada, T.; Hiraoka, T.; Hayamizu, Y.; Kakudate, Y.; Tanaike, O.; Hatori, H.; Yumura, M.; Iijima, S. *Nat. Mater.* **2006**, *5*, 987–994.
(10) Cao, A.; Dickrell, P. L.; Sawyer, W. G.; Ghasemi-Nejhad, M. N.; Ajayan, P. M. *Science* **2005**, *310*, 1307–1310.
(11) Tong, T.; Zhao, Y.; Delzeit, L.; Kashani, A.; Meyyappan, M.; Majumdar, A. *Nano Lett.* **2008**, *8*, 511–515.
(12) Deck, C. P.; Flowers, J.; McKee, G. S. B.; Vecchio, K. *J. Appl. Phys.* **2007**, *101*, No. 023512.
(13) Zbib, A. A.; Mesarovic, S. D.; Lilleodden, E. T.; McClain, D.; Jiao, J.; Bahr, D. F. *Nanotechnology* **2008**, *19*, 175704.
(14) Cerda, E.; Mahadevan, L. *Phys. Rev. Lett.* **2003**, *90*, No. 074302.
(15) Brangwynne, C. P.; MacKintosh, F. C.; Kumar, S.; Geisse, N. A.; Talbot, J.; Mahadevan, L.; Parker, K. K.; Ingber, D. E.; Weitz, D. A. *J. Cell Biol.* **2006**, *173*, 733–741.
(16) Johnson, K. L. *Contact Mechanics*; Cambridge University Press: Cambridge, U.K., 1985.
(17) Landau, L. D.; Lifshitz, E. M.; Kosevich, A. M.; Pitaevskii, L. P. *Theory of Elasticity: Course of Theoretical Physics*; Pergamon Press: Oxford, 1986.
(18) Schubert, B.; Majidi, C.; Groff, R. E.; Baek, S.; Bush, B.; Maboudian, R.; Fearing, R. S. *J. Adhes. Sci. Technol.* **2007**, *21*, 1297–1315.
(19) Cohen, A. E.; Mahadevan, L. *Proc. Natl. Acad. Sci. U.S.A.* **2003**, *100*, 12141–12146.
(20) Zhao, Y.; Tong, T.; Delzeit, L.; Kashani, A.; Meyyappan, M.; Majumdar, A. *J. Vac. Sci. Technol., B* **2006**, *24*, 331–335.
(21) Sethi, S.; Ge, L.; Ci, L.; Ajayan, P. M.; Dhinojwala, A. *Nano Lett.* **2008**, *8*, 822–825.
(22) Vaia, R.; Baur, J. *Science* **2008**, *319*, 420–421.

DOI: 10.1021/nl102398w | *Nano Lett.* **2010,** *10,* 4509–4513